Splicing of α_{1A} subunit gene generates phenotypic variants of P- and Q-type calcium channels

Emmanuel Bourinet[1], Tuck W. Soong[2,4], Kathy Sutton[2], Sarah Slaymaker[2], Eleanor Mathews[2], Arnaud Monteil[1], Gerald W. Zamponi[3], Joel Nargeot[1] and Terry P. Snutch[2]

[1] *Physiopathologie des Canaux Ioniques, IGH, CNRS UPR 1142, Montpellier, France*

[2] *Biotechnology Laboratory, University of British Columbia, Vancouver, British Columbia, Canada*

[3] *Department of Pharmacology, University of Calgary, Calgary, Alberta, Canada*

[4] *Present Address: Institute of Molecular and Cell Biology, 30 Medical Drive, University of Singapore, Singapore*

The first two authors contributed equally to this work

Correspondence should be addressed to T.P.S. (snutch@zoology.ubc.ca)

P-type and Q-type calcium channels mediate neurotransmitter release at many synapses in the mammalian nervous system. The α_{1A} calcium channel has been implicated in the etiologies of conditions such as episodic ataxia, epilepsy and familial migraine, and shares several properties with native P- and Q-type channels. However, the exact relationship between α_{1A} and P- and Q-type channels is unknown. Here we report that alternative splicing of the α_{1A} subunit gene results in channels with distinct kinetic, pharmacological and modulatory properties. Overall, the results indicate that alternative splicing of the α_{1A} gene generates P-type and Q-type channels as well as multiple phenotypic variants.

The electrophysiological and pharmacological diversity of native calcium (Ca^{2+}) channels (L, N, P, Q and T types) is well documented[1]. These subtypes have different functions; low-voltage-activated T-type channels shape action potentials and generate firing patterns[2], whereas L-type channels regulate Ca^{2+}-dependent genes and enzymes[3,4], and N-type and P/Q-type channels contribute to neurotransmitter release[5–8].

High-threshold neuronal Ca^{2+} channels are heterotrimeric complexes composed of a pore-forming α_1 subunit associated with β and $\alpha_2\delta$ subunits. Each of the cloned α_1 subunits has distinct functional characteristics that are modulated by co-expression of any of four β subunits[9]. Channels formed from α_{1C} and α_{1D} subunits have the properties of neuronal dihydropyridine-sensitive L-type channels, and α_{1B} channels encode ω-CgTx GVIA-sensitive N-type channels[9]. The α_{1E} channel shares some properties with both low-threshold channels (high sensitivity to nickel block, permeation $Ca^{2+} > Ba^{2+}$) and high-threshold Ca^{2+} channels (activation at more positive potentials, single-channel conductance > 10 pS)[10–12], although the native counterpart of this subunit remains unclear. T-type low-threshold channels are encoded by at least three different α_1 subunits (α_{1G}, α_{1H}, α_{1I}) and seem not to require β and $\alpha_2\delta$ subunits for functional expression[13,14].

P-type Ca^{2+} channels, originally described in cerebellar Purkinje cells[15], are widely distributed[16,17] and mediate neurotransmitter release in the central and peripheral nervous systems[5–8]. Q-type Ca^{2+} channels, first described in cerebellar granule cells[18,19], also mediate neurotransmitter release at some synapses[20]. Native P- and Q-type channels differ in sensitivity to ω-agatoxin IVA (ω-Aga IVA; K_d ~2 nM for P-type versus > 100 nM for Q-type) and in their inactivation kinetics. (P-type currents show a non-inactivating waveform during prolonged membrane depolarization, whereas Q-type currents show a pronounced inactivation.) Some native Ca^{2+} channels have properties related to but distinct from either P- or Q-type channels, suggesting a closely related family of channel types[21,22].

The α_{1A} subunit[23,24] is highly expressed in both Purkinje and cerebellar granule cells and shares several properties with both native P- and Q-type Ca^{2+} currents[25,26]. Mutations in the α_{1A} subunit result in several neuropathological conditions, including familial hemiplegic migraine, cerebellar ataxia and epilepsy[27–29]. The properties of α_{1A} do not exactly match those of either P- or Q-type Ca^{2+} currents, and there has also been no account for their distinct sensitivities to ω-Aga IVA. Here we report that alternative splicing at distinct sites within the α_{1A} subunit gene generate multiple types of P- and Q-type conductances that exhibit distinct gating, pharmacology and modulatory characteristics. We also suggest there is little reason that α_{1A} channels should be selectively subdivided into distinct P- versus Q- subtypes.

Results

α_{1A} isoforms are generated by alternative splicing

Screening of a rat brain cDNA library identified a calcium channel α_{1A} subunit (called $\alpha_{1A\text{-}b}$) that differed from the primary sequence of the original rat brain $\alpha_{1A\text{-}a}$ (ref. 24) at three sites (Fig. 1a). The domain I–II linker in $\alpha_{1A\text{-}b}$ contained a single valine insertion (Val_{421}) located 18 residues carboxyl to the β subunit binding site[30]. In domain IV, $\alpha_{1A\text{-}b}$ contained an insertion of two residues, Asp and Pro (N_{1605}-P_{1606}), in the

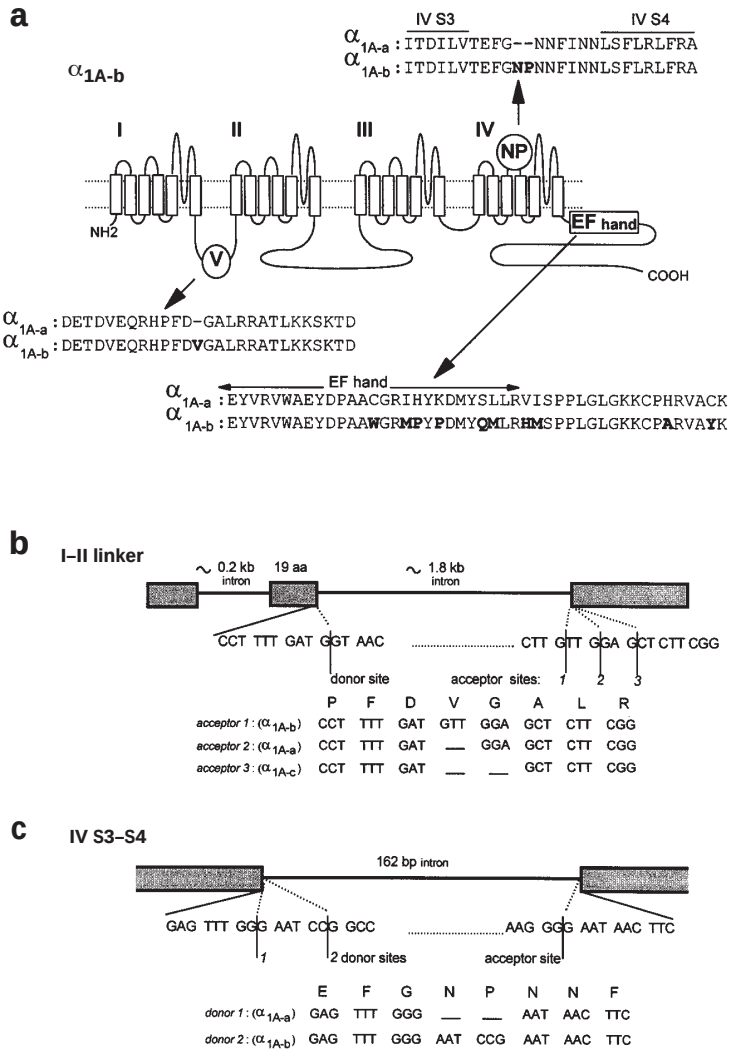

Fig. 1. Alternative splicing generates multiple α_{1A} isoforms. **(a)** Differences between $\alpha_{1A\text{-}a}$ and $\alpha_{1A\text{-}b}$ subunits (single-letter code). **(b)** Comparison of the α_{1A} genomic and cDNA sequences in the domain I–II linker identifies possible donor and acceptor sites. Exons are indicated by filled boxes and intron sequences by lines. **(c)** Comparison of the α_{1A} genomic and cDNA sequences in the domain IV S3–S4 region shows that a 162-bp intron separates two exons.

extracellular linker separating transmembrane segments S3 and S4. Finally, $\alpha_{1A\text{-}b}$ contained ten substituted residues in a stretch of thirty amino acids in the carboxyl tail adjacent to domain IV S6. Of the ten substitutions, six are located in a region highly similar to the divalent ion binding domain (EF hand) of Ca^{2+}-binding proteins[31].

To determine the molecular nature of these differences, we sequenced clones from a rat genomic library and also analyzed rat DNA by PCR. Clones corresponding to the region flanking the α_{1A} I–II linker had an Asp preceding the Val_{421} insertion (Fig. 1b). A 1.8-kb intron separated the Asp residue from downstream Gly_{422} found in $\alpha_{1A\text{-}a}$ transcripts. The flanking genomic and cDNA sequences contained a common 5′ splice donor site and three possible 3′ acceptor sites: one that would result in either the inclusion or exclusion of Val_{421}, another that would include Gly_{422}, and a third that could produce an α_{1A} variant lacking both the Gly and Val_{421} residues (Fig. 1b). To test this third possibility, we examined five additional α_{1A} cDNAs and found that one of five lacked both the Val_{421} and Gly_{422} residues (called $\alpha_{1A\text{-}c}$). To confirm that the $\alpha_{1A\text{-}c}$ variant was expressed *in vivo*, we examined total cerebellar and hippocampal RNAs by RT-PCR followed by DNA sequencing. Of 81 PCR products, 16% were the $\alpha_{1A\text{-}c}$ variant, 79% the domain I–II-linker $\alpha_{1A\text{-}a}$ isoform, and 5% the $\alpha_{1A\text{-}b}$ isoform (data not shown).

PCR amplification of rat genomic DNA across the domain IV S3–S4 region identified a 162-bp intron that when absent resulted in α_{1A} channels lacking N_{1605}-P_{1606} ($\alpha_{1A\text{-}a}$ variant), whereas inclusion of N_{1605}-P_{1606} (the α_{1Ab} isoform) resulted from use of an alternative 5′ splice donor site (Fig. 1c). The genomic nature of the differences between $\alpha_{1A\text{-}a}$ and α_{1Ab} in the EF hand region were not determined, although the 10 amino-acid substitutions are contained in a contiguous stretch of 90 bp with only 53% sequence identity, suggesting a mutually exclusive alternative splicing mechanism.

Differential expression of α_{1A} isoforms in the rat CNS

The spatial expression patterns of $\alpha_{1A\text{-}a}$ and α_{1Ab} in the rat CNS were examined by RT-PCR of the domain I–II linker region and by *in situ* hybridization using antisense oligonucleotide probes against the distinct EF hand sequences. Stringent PCR conditions allowed the selective amplification of $\alpha_{1A\text{-}b}$ variants containing the 3-bp Val_{421} insertion in the domain I–II linker (Fig. 2a). The expected $\alpha_{1A\text{-}b}$ 208-bp fragment was detected in all rat brain regions examined, indicating that α_{1A} transcripts containing Val_{421} are widely expressed. Furthermore, transcripts containing Val_{421} were also detected at moderate levels in kidney RNA (Fig. 2a). Attempts to amplify the 208-bp fragment from rat genomic DNA samples were unsuccessful, consistent with the presence of the intronic sequences in the α_{1A} I–II linker (see Fig. 1b).

In situ hybridization with the EF hand probes revealed differential expression of $\alpha_{1A\text{-}a}$ and $\alpha_{1A\text{-}b}$ transcripts. Most brain regions prominently expressed $\alpha_{1A\text{-}b}$. Expression of $\alpha_{1A\text{-}a}$ was strong in the cerebellar cortex, with lower levels in the cortex, hippocampus and olfactory tubercule (not shown). Both $\alpha_{1A\text{-}a}$ and $\alpha_{1A\text{-}b}$ were detected in cerebellar granule cells, with $\alpha_{1A\text{-}a}$ predominantly in Purkinje cells (Fig. 2b and c). In contrast, $\alpha_{1A\text{-}b}$ was highly expressed in CA1-CA3 pyramidal and dentate granule cells in the hippocampus, where $\alpha_{1A\text{-}a}$ expression was significantly lower (Fig. 2d and e).

Transcripts encoding α_{1A} variants with N_{1605}-P_{1606} contain an additional *Tfi* I restriction enzyme site. PCR amplication of rat cerebellar and hippocampal α_{1A} RNAs and digestion with *Tfi* I showed that both regions expressed both α_{1A} channel variants. However, in cerebellar RNA, most isoforms lacked N_{1605}-P_{1606}, whereas in hippocampus both forms were represented approximately equally (not shown).

α_{1A} splicing affects electrophysiological properties

The electrophysiological properties of $\alpha_{1A\text{-}a}$ and $\alpha_{1A\text{-}b}$ channels were compared by transient expression in *Xenopus* oocytes (co-expressed with rat brain $\alpha_2\delta$ and β_4 subunits). The $\alpha_{1A\text{-}b}$ iso-

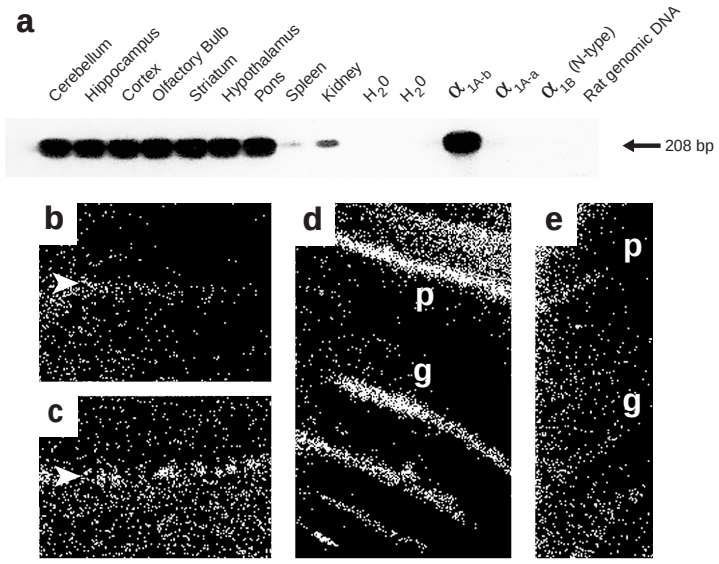

Fig. 2. Both $\alpha_{1A\text{-}a}$ and $\alpha_{1A\text{-}b}$ variants are expressed in the rat nervous system. **(a)** RT-PCR demonstrating the expression of $\alpha_{1A\text{-}b}$ transcripts. Blotting and hybridization of the PCR products with an internal oligonucleotide showed the specific amplification of an $\alpha_{1A\text{-}b}$ 208-bp fragment from the $\alpha_{1A\text{-}b}$ template cDNA control but not the $\alpha_{1A\text{-}a}$ cDNA. **(b–e)** *In-situ* hybridization to adult rat brain sections using radiolabeled oligonucleotide probes specific to the $\alpha_{1A\text{-}a}$ and $\alpha_{1A\text{-}b}$ EF hand regions. Sections show $\alpha_{1A\text{-}b}$ **(b)** and $\alpha_{1A\text{-}a}$ **(c)** in cerebellum and $\alpha_{1A\text{-}b}$ **(d)** and $\alpha_{1A\text{-}a}$ **(e)** in hippocampal CA1-CA3 pyramidal (p) and dentate granule cells (g).

form had three significant functional differences from $\alpha_{1A\text{-}a}$ (Fig. 3). First, $\alpha_{1A\text{-}b}$ inactivation rate was dramatically slowed, with 84 ± 3% (n = 12) of the whole-cell current remaining after a 400-ms test pulse compared to 39 ± 8% for $\alpha_{1A\text{-}a}$ (n = 8; Fig. 3a). After a 16-s test pulse, approximately 50% of the $\alpha_{1A\text{-}b}$ current remained, whereas $\alpha_{1A\text{-}a}$ currents were completely inactivated (Fig. 3b). Second, $\alpha_{1A\text{-}b}$ showed a significant ($p < 0.05$) positive shift in the current–voltage relationship by ~6 mV ($\alpha_{1A\text{-}a}$ $V_{0.5}$ = –4.1 ± 0.5, n = 18; $\alpha_{1A\text{-}b}$ $V_{0.5}$ = 2.1 ± 0.7, n = 20; Fig. 3a). Third, the voltage dependence of inactivation of $\alpha_{1A\text{-}b}$ was shifted more positively by ~20 mV. Furthermore, even after the holding potential was clamped to +50 mV for 15 s, ~60% of the whole-cell current was not inactivated (Fig. 3c).

Because co-expression of Ca^{2+} channel β subunits both alters channel kinetics and shifts the current–voltage relationship[9], we asked whether these functional differences were specific for neuronal β subunit types. The inactivation rate of $\alpha_{1A\text{-}b}$ was significantly slower than $\alpha_{1A\text{-}a}$ for all β subunits tested (Fig. 3b), regardless of whether the β subunit normally increases (β_{1b}) or decreases (β_{2a}) inactivation rates. Furthermore, regardless of the co-expressed β subunit, the current–voltage relationship of $\alpha_{1A\text{-}b}$ was significantly ($p < 0.05$) more positive when compared to $\alpha_{1A\text{-}a}$ (not shown). The amino-acid differences in $\alpha_{1A\text{-}b}$ were not associated with significant changes in other channel properties examined, including ion permeation (not shown), the rate of activation (not shown) and the slope of the current–voltage relationship ($\alpha_{1A\text{-}a}$, k = –3.5 ± 0.2, n = 18; $\alpha_{1A\text{-}b}$, k = –3.7 ± 0.5, n = 20).

Val_{421} and N_{1605}-P_{1606} differentially affect properties

To identify the regions of $\alpha_{1A\text{-}b}$ responsible for its distinct gating characteristics, we constructed chimeras between $\alpha_{1A\text{-}a}$ and $\alpha_{1A\text{-}b}$ (Fig. 4a). The $\alpha_{1A\text{-}a}$ (+V) chimera was identical to $\alpha_{1A\text{-}a}$ except for the Val_{421} insertion in the domain I–II linker, and the $\alpha_{1A\text{-}b}$ (–V) chimera differed from $\alpha_{1A\text{-}a}$ only by insertion of N_{1605}-P_{1606} and substitution of the $\alpha_{1A\text{-}b}$ EF hand region. The $\alpha_{1A\text{-}b}$ (–V) chimera showed fast inactivation kinetics similar to those of $\alpha_{1A\text{-}a}$ (42 ± 3% remaining after 400 ms, n = 9) but retained a current–voltage relationship positively shifted by ~6 mV ($V_{0.5}$ = 2.7 ± 0.5, n = 19; Fig. 3a). In contrast, the $\alpha_{1A\text{-}a}$ (+V) chimera had slow inactivation kinetics similar to that of $\alpha_{1A\text{-}b}$ (79 ± 3% remaining after 400 ms, n = 13) and a relatively negative current–voltage relationship similar to $\alpha_{1A\text{-}a}$ ($V_{0.5}$ = –5.0 ± 0.3, n = 21; Fig. 3a).

We examined two additional chimeras: $\alpha_{1A\text{-}a}$ (+NP), which was identical to $\alpha_{1A\text{-}a}$ except for the insertion of N_{1605}-P_{1606}, and $\alpha_{1A\text{-}b}$ (–NP), which was identical to $\alpha_{1A\text{-}b}$ except that it lacked N_{1605}-P_{1606} (Fig. 4a). Inactivation properties of $\alpha_{1A\text{-}a}$ (+NP) were identical to those of $\alpha_{1A\text{-}a}$, although $V_{0.5}$ was shifted similarly to $\alpha_{1A\text{-}b}$ ($\alpha_{1A\text{-}a}$ (+NP) = 3.3 ± 0.4, n = 11). In contrast, the $\alpha_{1A\text{-}b}$ (–NP) chimera had negatively shifted $V_{0.5}$ but slow inactivation kinetics typical of the wild-type $\alpha_{1A\text{-}b}$ ($\alpha_{1A\text{-}b}$ (–NP) = –3.9 ± 0.4, n = 12). Another chimera containing the $\alpha_{1A\text{-}c}$ variation in the domain I–II linker ($\alpha_{1A\text{-}a}$ missing both Val_{421} and Gly_{422}) showed similar waveform and inactivation properties to $\alpha_{1A\text{-}a}$ and was not examined further in the present study (not shown). We could not detect any distinct contributions of the spliced EF hand regions to any of the Ca^{2+} channel properties examined in this study.

Presence or absence of Val_{421} affects inactivation

Cell-attached, single-channel recordings were made in oocytes expressing either the $\alpha_{1A\text{-}a}$ or the $\alpha_{1A\text{-}a}$ (+V) chimera. At the single-channel level, the presence of Val_{421} caused the appearance of multiple bursts of channel activity (Fig. 4b), which continued throughout test pulses as long as 24 s (not shown). Ensemble averages of sweeps with unitary activity showed a rapidly inactivating $\alpha_{1A\text{-}a}$ current, whereas $\alpha_{1A\text{-}a}$ (+V) averaged currents were sustained (Fig. 4b). Varying the holding potential from –100 to –20 mV completely inactivated $\alpha_{1A\text{-}a}$ channels but did not affect $\alpha_{1A\text{-}a}$ (+V) open probability, consistent with the lack of complete steady-state inactivation at the whole-cell level (not shown).

Comparison of the open-time distributions for $\alpha_{1A\text{-}a}$ and $\alpha_{1A\text{-}a}$ (+V) channels (Fig. 4c) shows that $\alpha_{1A\text{-}a}$ openings are characterized by two apparent brief open states (0.34 and 1.33 ms), whereas the $\alpha_{1A\text{-}a}$ (+V) distribution had three markedly longer open states (0.90, 3.26 and 15.74 ms) . Thus, Val_{421} contributes to two separate effects: destabilization of the inactivated state, as indicated by the appearance of multiple bursts, and stabilization of the open state(s), as indicated by the increase in mean open time and appearance of an additional time constant. There was no significant change in the single-channel slope conductance of α_{1A} channels with or without Val_{421} (not shown; $\alpha_{1A\text{-}a}$, 16.5 ± 0.4 pS, $\alpha_{1A\text{-}a}$(+V), 17.2 ± 0.7 pS; $p < 0.05$, n = 4).

N_{1605}-P_{1606} reduces ω-agatoxin IVA sensitivity

The major distinguishing characteristic between native P- and Q-type calcium currents is their differential sensitivity to the spider peptide toxin ω-Aga IVA[8,16–19]. In *Xenopus* oocytes, $\alpha_{1A\text{-}a}$ and $\alpha_{1A\text{-}b}$ channels were blocked approximately equally by 200

nM ω-Aga IVA (~25% block) and by 5 μM ω-CTx-MVIIC (~80% block; Fig. 5a). In contrast to native P-type channels, ω-Aga IVA block was not reversed by application of depolarizing prepulses (data not shown). However, in transfected human embryonic kidney (HEK 293) cells, 100 to 300 nM ω-Aga IVA completely blocked the wild-type $\alpha_{1A\text{-}a}$ (Fig. 5b and c). As for native P-type channels, block was relieved by a series of strong depolarizations (Fig. 5b). The sensitivity of $\alpha_{1A\text{-}a}$ to ω-Aga IVA was markedly reduced in channels containing N_{1605}-P_{1606} in domain IV S3–S4 (Fig. 5c). The N_{1605}-P_{1606} insertion lowered the blocking rate constant, k_{on}, 7-fold ($\alpha_{1A\text{-}a}$ = 6.475 × 10^{-3} $\mu M^{-1}s^{-1}$; $\alpha_{1A\text{-}a}$ (+NP) = 0.9198 × 10^{-3} $\mu M^{-1}s^{-1}$) and increased k_{off} 2-fold ($\alpha_{1A\text{-}a}$ = 1.47 × 10^{-3} s^{-1}; $\alpha_{1A\text{-}a}$ (+NP) = 3.045 × 10^{-3} s^{-1}), resulting in an 11-fold decrease in affinity for ω-Aga IVA (Fig. 5d and e; K_d for $\alpha_{1A\text{-}a}$ =14.8 nM; K_d for $\alpha_{1A\text{-}a}$ (+NP) = 167 nM). In contrast to ω-Aga IVA, the snail peptide toxin ω-CTx-MVIIC blocked both $\alpha_{1A\text{-}a}$ and $\alpha_{1A\text{-}a}$ (+NP) with a similar time course and potency (Fig. 5f). These pharmacological profiles in HEK cells suggest that native P-type channels lack N_{1605}-P_{1606}, whereas Q-type channels contain these two residues.

G proteins and PKC modulate α_{1A} splice variants

The activation of certain neurotransmitter receptors inhibits P/Q-type Ca^{2+} channels through the binding of G-protein βγ subunits directly to the α_{1A} domain I–II linker[32]. G-protein modulation of Ca^{2+} channels characteristically involves decreased whole-cell currents, slowed activation and inactivation kinetics, and relief from inhibition by application of positive prepulses (called facilitation)[33]. Because Val_{421} is located in one of two $G_{\beta\gamma}$ binding sites of the I–II linker and may directly alter $G_{\beta\gamma}$ binding affinity, we tested whether this residue affects the G-protein-dependent modulation of α_{1A} channels. The μ-opioid receptor agonist DAMGO inhibited both $\alpha_{1A\text{-}a}$ and $\alpha_{1A\text{-}b}$ currents in cells co-expressing the μ-opioid receptor (Fig. 6). However, DAMGO-inhibited $\alpha_{1A\text{-}b}$ activation kinetics were significantly more slowed and the overall opioid-induced inhibition more pronounced compared with $\alpha_{1A\text{-}a}$ (Fig. 6a). Times to peak indicated that Val_{421} is responsible for the slowed kinetics of $\alpha_{1A\text{-}b}$ after G-protein activation (Fig. 6a). In the presence of DAMGO, the two splice variants also showed distinct magnitudes of voltage-dependent facilitation as determined by applying a 50-ms prepulse to +150 mV before a test pulse from –100 mV to + 10 mV. When measured 20 ms after the test pulse, the $\alpha_{1A\text{-}b}$ variant showed twofold more facilitation ($\alpha_{1A\text{-}b}$, 22 ± 3%, n = 15; $\alpha_{1A\text{-}a}$, 10 ± 2%, n = 14; data not shown). Furthermore, varying the time between the prepulse and the test pulse showed that the $\alpha_{1A\text{-}a}$-facilitated currents were re-inhibited more rapidly compared to $\alpha_{1A\text{-}b}$ (Fig. 6b; τ reinhibition $\alpha_{1A\text{-}a}$ = 25 ± 2 ms, n = 15; $\alpha_{1A\text{-}a(+V)}$, 39 ± 3, n = 14). The difference in re-inhibition kinetics following DAMGO-induced G-protein inhibition is due to Val_{421} in the domain I–II linker (Fig. 6b).

The stimulation of protein kinase C (PKC) with phorbol esters upregulates $\alpha_{1A\text{-}a}$ currents by ~10% (Fig. 6c). Because the domain I–II linker contributes to the PKC-dependent upregulation of some neuronal calcium chan-

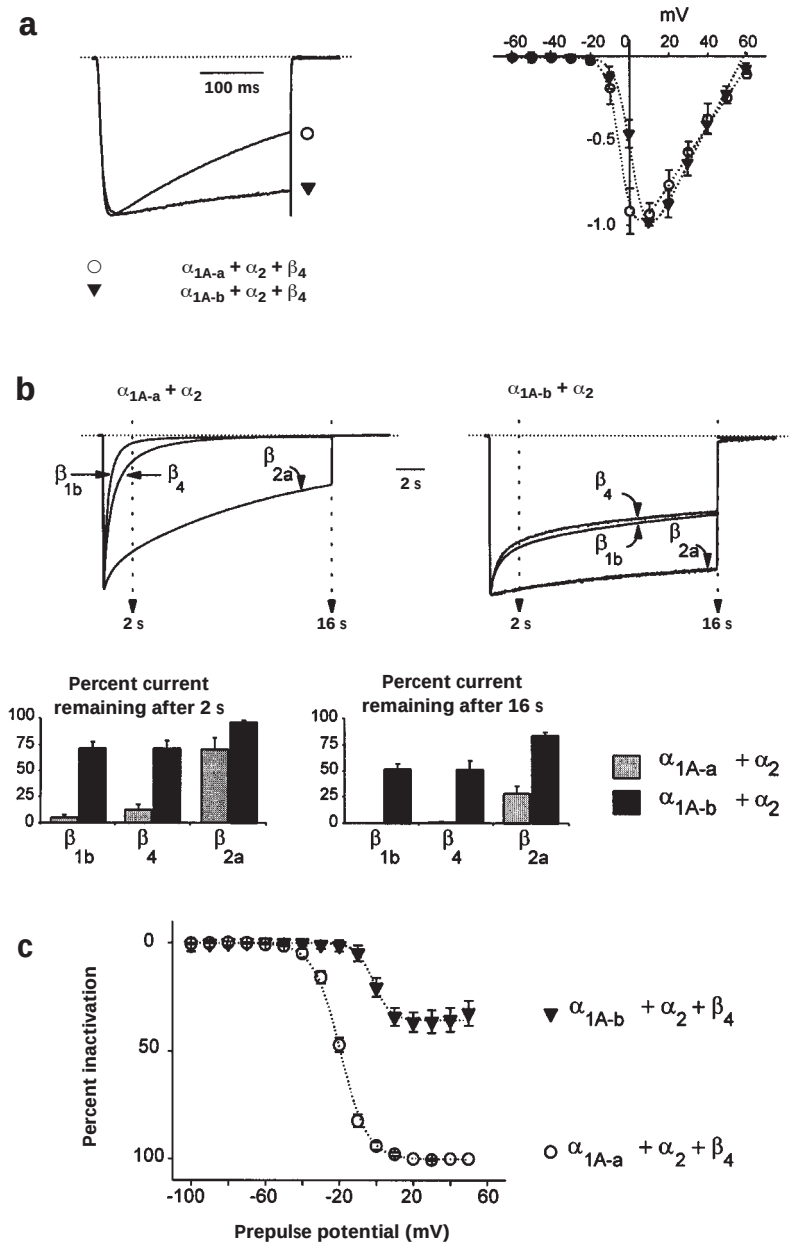

Fig. 3. $\alpha_{1A\text{-}a}$ and $\alpha_{1A\text{-}b}$ have distinct functional properties. **(a)** Waveforms and current–voltage relationships for $\alpha_{1A\text{-}a}$ and $\alpha_{1A\text{-}b}$. Waveforms of peak normalized current from a holding potential of –100 mV show that $\alpha_{1A\text{-}b}$ barely inactivates over 400 ms. The mean normalized *I–V* curves for $\alpha_{1A\text{-}a}$ (n = 18) and $\alpha_{1A\text{-}b}$ (n = 20) show a positive shift for $\alpha_{1A\text{-}b}$. **(b)** Normalized waveforms for $\alpha_{1A\text{-}a}$ and $\alpha_{1A\text{-}b}$ channels co-expressed with three different Ca^{2+} channel β subunits. Cells were depolarized from a holding potential of –100 mV to the peak *I–V* potential, and the currents remaining after 2 s or 16 s were averaged and presented as histograms (mean, n = 8–17 cells for each combination). **(c)** Steady-state inactivation curves for $\alpha_{1A\text{-}a}$ and $\alpha_{1A\text{-}b}$ co-expressed with β_4 and α_2. Cells were held at various potentials for 16 s before a test pulse to +10 mV. The half-inactivation potentials obtained from the fit were –17.2 ± 0.7 mV (n = 5) for $\alpha_{1A\text{-}a}$ and –1.6 ± 0.8 mV (n = 10) for $\alpha_{1A\text{-}b}$.

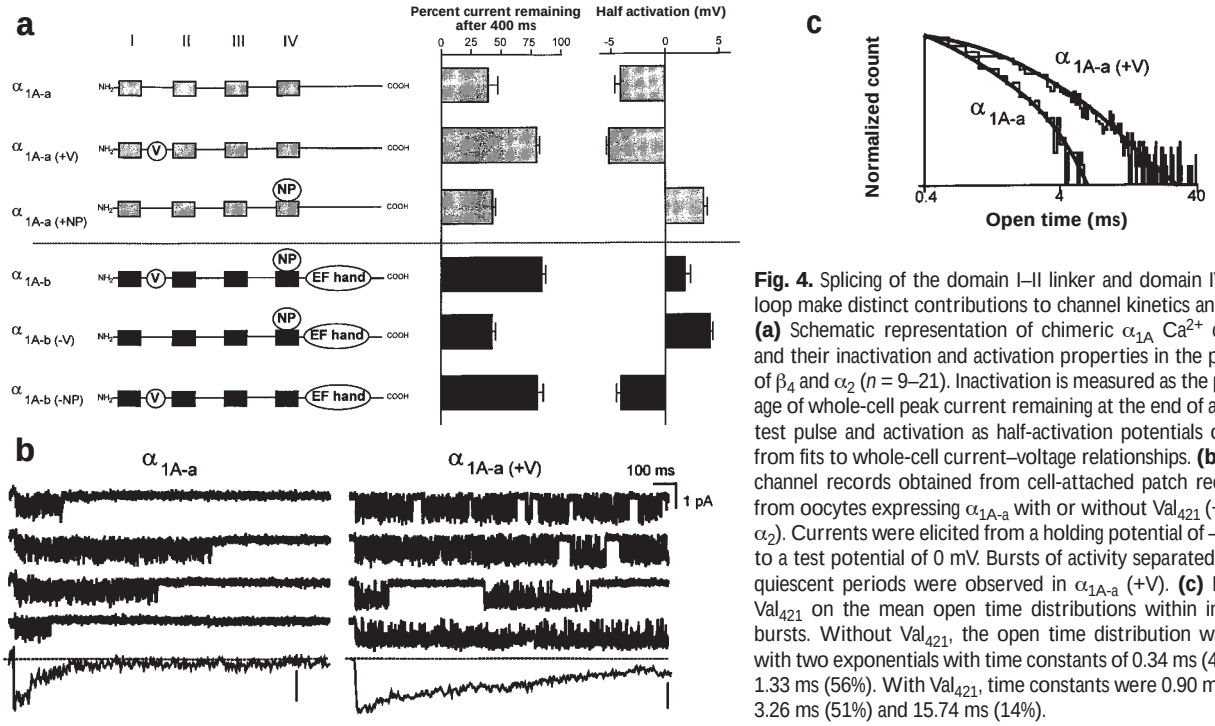

Fig. 4. Splicing of the domain I–II linker and domain IV S3–S4 loop make distinct contributions to channel kinetics and gating. **(a)** Schematic representation of chimeric α_{1A} Ca^{2+} channels and their inactivation and activation properties in the presence of β_4 and α_2 (n = 9–21). Inactivation is measured as the percentage of whole-cell peak current remaining at the end of a 400-ms test pulse and activation as half-activation potentials obtained from fits to whole-cell current–voltage relationships. **(b)** Single-channel records obtained from cell-attached patch recordings from oocytes expressing $\alpha_{1A\text{-}a}$ with or without Val_{421} (+ β_4 and α_2). Currents were elicited from a holding potential of –100 mV to a test potential of 0 mV. Bursts of activity separated by brief quiescent periods were observed in $\alpha_{1A\text{-}a}$ (+V). **(c)** Effect of Val_{421} on the mean open time distributions within individual bursts. Without Val_{421}, the open time distribution was fitted with two exponentials with time constants of 0.34 ms (44%) and 1.33 ms (56%). With Val_{421}, time constants were 0.90 ms (35%), 3.26 ms (51%) and 15.74 ms (14%).

nels[34], we compared the modulation of $\alpha_{1A\text{-}a}$ and $\alpha_{1A\text{-}b}$ variants. Phorbol ester (PMA, 100 nM) caused twofold more upregulation of $\alpha_{1A\text{-}b}$ channels than of $\alpha_{1A\text{-}a}$ (+PMA $\alpha_{1A\text{-}a}$, 1.10 ± 0.01, +PMA $\alpha_{1A\text{-}b}$, 1.24 ± 0.03; Fig. 6c). The presence of Val_{421} in the domain I–II linker was responsible for conferring the higher degree of upregulation associated with $\alpha_{1A\text{-}b}$ channels (Fig. 6d). Overall, the results support the notion that the domain I–II linker is a crucial determinant for PKC and $G_{\beta\gamma}$ modulation[32] and suggest alternative splicing as a mechanism for controlling the second-messenger-dependent modulation of neuronal Ca^{2+} channels.

Discussion

Alternative splicing alters channel properties

Our present understanding of Ca^{2+} channel structure–function relationships primarily results from chimeric cDNA and mutagenesis studies, which have identified regions of Ca^{2+} channel α_1 subunits important for permeation[35], activation[36] and inactivation[37], excitation–contraction coupling[38] and β subunit binding[30]. The functional effect of alternative splicing is an important tool because it provides insights into native amino acids essential for controlling channel properties.

Here we show that alternative splicing of the rat α_{1A} gene results in variants with relatively small alterations in the domain I–II linker and domain S3–S4 regions. Two apparently distinct channel properties are affected by alternative splicing of N_{1605}-P_{1606} in domain IV 53-54. The approximately 6-mV shift in current–voltage relationships associated with N_{1605}-P_{1606} is consistent with studies on L-type Ca^{2+} channels showing that mutations both within and flanking S3 segments affect the voltage dependence of activation[36]. Many native Ca^{2+} channels display variable activation characteristics, which may generally result from alternative splicing in S3–S4 regions.

The second major change in channel properties associated with N_{1605}-P_{1606} is to alter the sensitivity of α_{1A} to the spider peptide toxin, ω-Aga IVA. ω-Aga IVA is a 48-residue positively charged peptide isolated from the venom of the funnel web spider *Agelenopsis aperta*, which has long been used as a diagnostic for native P/Q-type Ca^{2+} channels[16,17]. As in native P-type currents, block of both $\alpha_{1A\text{-}a}$ and $\alpha_{1A\text{-}b}$ variants by ω-Aga IVA in HEK cells was highly voltage sensitive and was reversed by application of positive prepulses. The major effects of the insertion of N_{1605}-P_{1606} were to decrease k_{on} and increase k_{off}, which together decreased toxin affinity 11-fold. Both ω-Aga IVA and ω-CTx MVIIC act extracellularly to block P/Q-type channels, although by distinct blocking mechanisms; ω-CTx MVIIC acts as a traditional pore blocker (S.I. McDonough, I.M. Mintz & B.P. Bean *Soc. Neurosci. Abstr.* 21, 140.9, 1995) and ω-Aga IVA binds to the gating machinery to stabilize channel closed states[39]. In contrast to ω-Aga-IVA, the presence or absence of N_{1605}-P_{1606} did not alter the block of α_{1A} channels by ω-CTx MVIIC, which is consistent with these toxins' different mechanisms of action.

ω-Aga IVA belongs to a class of polypeptide neurotoxins that act via a common mechanism to alter the gating properties of voltage-gated ion channels. These include α and β scorpion toxins (Na^+ channels)[40,41], hanatoxin (K^+ channels)[42] and grammotoxin (Ca^{2+} channels)[43]. Our data are consistent with studies showing that peptide gating modifiers interact at a conserved structural gating modifier site that primarily includes S3–S4 loops. Single amino-acid changes in the domain II S3–S4 loop of Na^+ channels and the S3–S4 loop of K^+ channels significantly alter toxin affinities[40–43]. In this regard, the insertion of N_{1605}-P_{1606} in α_{1A} by splicing may alter the conformation of the domain S3–S4 loop and result in an unfavorable binding site for ω-Aga IVA.

The third change in α_{1A} properties associated with alternative splicing is that the presence of Val_{421} dramatically slowed channel inactivation kinetics and affected steady-state inactivation. The Val_{421} residue is close to the site in the domain I–II linker that interacts with Ca^{2+} channel β subunits[30]. However, Val_{421} is

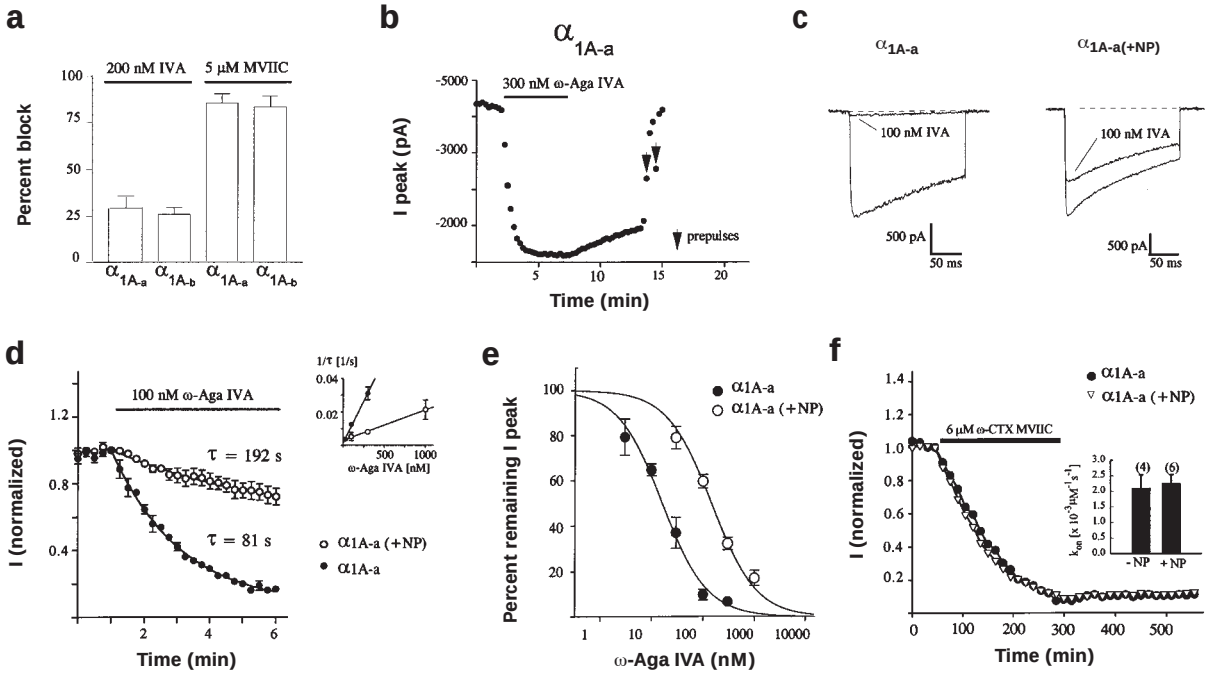

Fig 5. Sensitivities of $\alpha_{1A\text{-}a}$ and $\alpha_{1A\text{-}a}$ (+NP) to ω-Aga-IVA and ω-CTx-MVIIC. **(a)** Whole-cell current records obtained from $\alpha_{1A\text{-}a}$ and $\alpha_{1A\text{-}b}$ (expressed transiently in *Xenopus* oocytes) after application of 200 nM ω-Aga-IVA or 6 μM ω-CTx-MVIIC. Mean ± s.e.; n = 5–8. **(b–f)** Channels expressed transiently in HEK cells. **(b)** Time course of development of ω-Aga IVA (300 nM) block of $\alpha_{1A\text{-}a}$ and reversal of toxin action with repetitive depolarizations (10 × 10 ms steps to +120 mV at 1 Hz). Test pulses to 0 mV were elicited from a holding potential of –100 mV every 15 seconds. **(c)** Whole-cell current records obtained from $\alpha_{1A\text{-}a}$ and $\alpha_{1A\text{-}a}$ (+NP) with or without 100 nM ω-Aga IVA. **(d)** Average normalized time course comparing the rate of development of ω-Aga IVA (300 nM) block of $\alpha_{1A\text{-}a}$ and $\alpha_{1A\text{-}a}$ (+NP). Inset, on-rate of block for $\alpha_{1A\text{-}a}$ and $\alpha_{1A\text{-}a}$ (+NP) varies linearly with ω-Aga IVA concentration. Mean data (± s.e.; n = 3–5) were fit according to the equation $1/\tau_{on} = k_{on}$ [ω-Aga IVA] + k_{off}. The K_d values were 14.8 nM for $\alpha_{1A\text{-}a}$ and 167 nM for $\alpha_{1A\text{-}a}$ (+NP). **(e)** Dose dependence of the effects of ω-Aga IVA for $\alpha_{1A\text{-}a}$ and $\alpha_{1A\text{-}a}$ (+NP). The solid lines reflect a fit with the Hill equation with the Hill coefficient arbitrarily held at 1.0. The IC_{50} values obtained were 16.3 nM for $\alpha_{1A\text{-}a}$ and 146 nM for $\alpha_{1A\text{-}a}$ (+NP). **(f)** Time course of development of ω-CTx-MVIIC (6 μM) block of $\alpha_{1A\text{-}a}$ and $\alpha_{1A\text{-}a}$ (+NP). Inset, blocking rate constants obtained for $\alpha_{1A\text{-}a}$ and $\alpha_{1A\text{-}a}$ (+NP). Test pulses to +10 mV were elicited from a holding potential of –100 mV every 15 seconds.

unlikely to affect inactivation by disrupting β subunit binding because all β subunits still shifted α_{1A} current–voltage properties. Furthermore, co-expression with the β_{2a} subunit, which normally slows inactivation, caused an additional significant slowing of $\alpha_{1A\text{-}b}$ currents. The presence of Val_{421} altered channel gating as reflected by these channels reopening throughout the depolarization. Assuming that Val_{421} alters the prevalence of different gating modes, these channels might enter an alternate mode with an increased rate constant for returning to the open state from the inactivated state. This less-stable inactivated state would be reflected in reopening during the depolarization.

The demonstration that the domain I–II linker contributes to Ca^{2+} channel inactivation[44] (Fig. 4) is distinct from studies of chimeric Ca^{2+} channels that suggested a predominant role for domain I in inactivation[37]. Although we did not detect any functional properties that could be attributed to alternative splicing of the EF hand region, it is unlikely that the specific splicing of this highly conserved structural motif is benign. Some possibilities include the interaction of this putative divalent ion binding site with intracellular cations, or the differential interaction at this site of yet-to-be identified proteins that bind to the Ca^{2+} channel carboxyl terminus.

Differential expression of α_{1A} splice variants

P-type currents originally described in cerebellar Purkinje cells can be distinguished from Q-type currents in cerebellar granule cells by their higher sensitivity to ω-Aga-IVA and non-inactivating waveform[15–19]. We showed that α_{1A} channels can exhibit the slower inactivation kinetics typically associated with P-type currents by associating with a co-expressed β_{2a} subunit, possessing Val_{421} in the domain I–II linker, or both (Fig. 2b). In contrast, α_{1A} channels lacking Val_{421} or associated with β_1, β_3 or β_4 subunits exhibit the faster inactivation kinetics typically associated with Q-type currents (Fig. 2b). The β_{2a} subunit is highly expressed in cerebellar Purkinje cells (data not shown); therefore the non-inactivating P-type currents may be encoded by the combination of $\alpha_{1A\text{-}a}$ and β_{2a} (and $\alpha_2\delta$).

α_{1A} transcripts both with and without N_{1605}-P_{1606} in domain IV S3–S4 were expressed at approximately equal levels in the hippocampus. In contrast, most α_{1A} transcripts in the cerebellum lacked N_{1605}-P_{1606}. The presence of variants that confer the lower Q-type and higher P-type affinities for ω-Aga IVA (Fig. 5) predicts that both P-type and Q-type channels are widely expressed in the hippocampus, as reported in CA1-CA3 cells[17,20]. The data also predict that most α_{1A} transcripts in the cerebellum would have the P-type pharmacological profile, as reported in Purkinje cells[21]. The more abundant cerebellar granule cells also highly express an inactivating Ca^{2+} current (called G1) with P-type pharmacology[21], although some controversy remains regarding the nature of Q-type currents in granule cells. The Q-type current originally described in cultured cerebellar granule cells was reported to represent up to 35% of the whole-cell Ca^{2+} current[19].

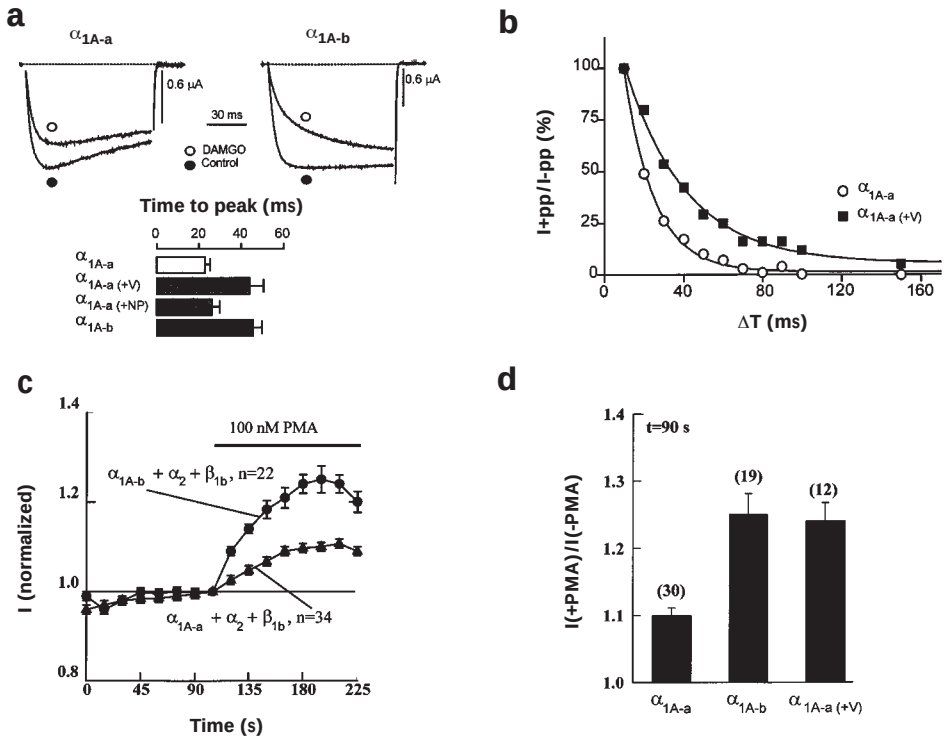

Fig. 6. Differential modulation of α_{1A} splice variants by G proteins and PKC. **(a, b)** Modulation of α_{1A-a} and α_{1A-b} by G proteins through the activation of a co-expressed μ-opioid receptor. **(a)** Currents elicited from a holding potential of –100 mV to a test potential of +10 mV with or without 1 μM DAMGO. Time-to-peak measurement shows that Val_{421} is responsible for the slower kinetics of α_{1A-b} following μ-opioid receptor activation. **(b)** Time course of reinhibition of the channels by G-proteins after temporary relief with a strong depolarizing prepulse to +150 mV. The presence of Val_{421} slows the reinhibition kinetics, suggesting a lower affinity of the channel for $G_{\beta\gamma}$. **(c, d)** Activation of PKC-dependent phosphorylation by application of 100 nM PMA. PKC-dependent upregulation of α_{1A-a} and α_{1A-b} follows a similar time course **(c)**, but the presence of Val_{421} causes a twofold increase in the upregulation **(c, d)**. In **(a)**, α_{1A} was co-expressed with β_4 and α_2 in *Xenopus* oocytes. In **(b–d)**, α_{1A} was co-expressed with β_4 and α_2 in HEK 293 cells.

However, others[21] failed to identify a Q-type current in this same primary granule cell preparation, but instead described the G1 current. One possible explanation for these conflicting results is that variations in culture conditions differentially induce expression of α_{1A-a} and α_{1A-b} splice variants in cultured granule cells.

ω-Aga-IVA affinity and expression system considerations

In *Xenopus* oocytes, the currents from cloned α_{1A} variants lacking N_{1605}-P_{1606} (α_{1A-a}) seem pharmacologically similar to native Q-type currents (K_d for ω-Aga-IVA > 100 nM; Fig. 5a)[29,30]. However, in HEK 293 cells, the K_d for ω-Aga IVA block of α_{1A-a} was approximately 15 nM. In another study[45], the identical rat brain α_{1A-a} cDNA expressed in COS cells was found to have a K_d of ~11 nM. This 15–20-fold difference in ω-Aga IVA sensitivity between mammalian cells and *Xenopus* oocytes may reflect cell-type-specific proteins that interact directly or indirectly with α_{1A-a} and alter pharmacological properties. Alternatively, cell-type-specific post-translational processing might alter channel affinity for ω-Aga IVA. For example, cloned acetycholine receptors (nAChR) expressed in *Xenopus* oocytes are incorrectly glycosylated compared to native nAChRs in *Torpedo* electroplax[46]. Because ω-Aga IVA is highly positively charged, the amounts and types of oligosaccharides (for example, high mannose versus complex) in the vicinity of the binding site may significantly affect toxin binding. Small differences in glycosylation patterns between mammalian cell lines and cerebellar Purkinje cells might also account for the difference in K_d between exogenously expressed α_{1A-a} ($K_d \approx 11$–15 nM) and native P-type currents ($K_d \approx 2$ nM).

Alternative splicing: physiological consequences

It is important to gain an understanding of the contributions of α_{1A} channels not only to normal neuronal functions, such as neurotransmitter release[5–8,20], but also to pathological states such as migraine, ataxia and epilepsy[27–29]. Immunohistochemical staining localizes α_{1A} calcium channels postsynaptically on cell bodies and dendrites as well as on presynaptic terminals[47]. In nerve terminals, both the 6-mV shift in α_{1A} channel activation resulting from the splicing of N_{1605}-P_{1606} and the slowed inactivation kinetics associated with Val_{421} would be predicted to alter the efficacy of synaptic transmission and significantly affect excitability.

Certain G-protein-coupled receptors inhibit P/Q-type and N-type channels by direct binding of $G_{\beta\gamma}$ to the domain I–II linker of α_{1A} and α_{1B} subunits[32]. The alternatively spliced Val_{421} residue is within one of two $G_{\beta\gamma}$ binding sites in the I–II linker, and its presence significantly increases slowing of the kinetics of G-protein-dependent inhibition and increases the overall degree of block (Fig. 6a and b). For both α_{1A-a} and α_{1A-b}, the kinetics of G-protein re-inhibition following a positive prepulse were well described by a single exponential. However, the time constant for re-inhibition was twice as long for α_{1A-b} (and α_{1A-a} + Val_{421}) as for α_{1A-a}. Within the few milliseconds of an action potential, the G-protein-inhibited α_{1A-b} channels with their very slow activation (Fig. 6a) would be more effectively inhibited, and their ability to trigger fast neurotransmitter release might be attenuated compared with α_{1A-a}. Similar to strong step depolarizations, bursts of action potentials can relieve G-protein inhibition[48]. Thus, the slower inhibition of α_{1A-b} channels would be expected to result in a substantially larger amount of calcium influx compared to α_{1A-a} (see Fig. 6b) and might cause more pronounced synaptic efficiency for slow neurotransmitter release.

P-, Q- or other types?

The four different types of Ca^{2+} channel β subunits are widely expressed in the rat CNS and also have subtype-specific expres-

sion patterns. Because each of the β subunits can differentially modify α_{1A} inactivation kinetics[25], inactivation kinetics are a poor diagnostic of Ca^{2+} channel subtype without knowledge of biochemical composition. Similarly, we find significant differences in the sensitivity of α_{1A} channels to ω-Aga IVA based on alternative splicing and the cell type used for expression. Thus, ω-Aga IVA affinity might not always be a reliable diagnostic of specific α_{1A} variants.

It is important to emphasize that the electrophysiological and pharmacological properties of the $\alpha_{1A\text{-}a}$ and $\alpha_{1A\text{-}b}$ variants described here do not exactly match those of either prototypical P-type or Q-type currents. Indeed, $\alpha_{1A\text{-}a}$ and $\alpha_{1A\text{-}b}$ describe two types of Ca^{2+} channels that exhibit some characteristics of both P-type and Q-type currents. Native Ca^{2+} channels with properties intermediate between P- and Q-type have been described in neurons and endocrine cells[21,22,49]. For example, the cerebellar granule cell G1 Ca^{2+} channel is highly sensitive to ω-Aga-IVA (similar to P-type) yet exhibits substantial inactivation (similar to Q-type)[21]. We predict that G1 is likely to be encoded by a splice variant missing both Val_{421} and N_{1605}-P_{1606} (for example, $\alpha_{1A\text{-}a}$).

The $\alpha_{1A\text{-}a}$ and $\alpha_{1A\text{-}b}$ variants examined here were each derived from single cDNAs; thus their properties likely reflect some portion of native α_{1A} Ca^{2+} currents. In addition, other α_{1A} variants are expressed that exhibit both some combination of the alternatively spliced regions examined here as well as other independent alternatively spliced sequences[23,27–29,49,50]. Assuming a mutually exclusive splicing mechanism, our data suggest that Q-type channels represent only one possible phenotypic variant resulting from splicing of a single α_{1A} gene encoding the P-type Ca^{2+} channel.

Methods

Electrophysiological recording. Preparation of *Xenopus* oocytes, nuclear injection with Ca^{2+} channel subunit cDNAs, two-microelectrode voltage clamp, and cell-attached single-channel, patch-clamp recordings were done as described[25,34]. For macroscopic currents, the bathing medium contained 40 mM $Ba(OH)_2$, 25 mM TEA-OH, 25 mM NaOH, 2 mM CsOH and 5 mM HEPES (titrated to pH 7.3 with methane-sulfonic acid). During voltage-clamp recordings, oocytes were routinely injected with BAPTA to eliminate the endogenous oocyte Ca-dependent chloride current. For G-protein modulation, Ca^{2+} channels were co-expressed with the μ-opioid receptor and G-protein activation was triggered via application of 1 μM DAMGO. For PKC modulation, oocytes were perfused with 100 nM PMA as described[34], and BAPTA was omitted.

For the determination of current–voltage relationships, curves were fitted according to the equation $I = G \times (V - E)/[1 + \exp((V - V_{0.5})/k)]$, where I is the current at a given voltage V, G is the conductance, E is the extrapolated reversal potential, $V_{0.5}$ is the voltage for half activation and k is the slope factor. For steady-state inactivation, cells were held at various potentials for 15 s and currents recorded during a subsequent test pulse to the peak potential of the *I–V*. Steady-state inactivation was calculated with a Boltzmann equation and the potential for half inactivation determined from the best fit. All values are given as mean ± s.e. Leak currents and capacitive transients were subtracted using a P/5 procedure.

Transient transfection of human embryonic kidney cells (HEK-tsa201) was done by standard calcium-phosphate precipitation, and whole-cell patch-clamp recordings were as described[48]. The external recording solution was 5 mM $BaCl_2$, 1 mM $MgCl_2$, 10 mM HEPES, 40 mM TEACl, 25 mM glucose and 65 mM CsCl (pH 7.2). The internal pipette solution was 105 mM CsCl, 25 mM TEACl, 1 mM $CaCl_2$, 11 mM EGTA and 10 mM HEPES (pH 7.2). Peptide toxins were perfused onto the cells using a gravity-driven microperfusion system.

Molecular biology. To identify the $\alpha_{1A\text{-}b}$ cDNA, we screened a rat brain cDNA library[24] with a [^{32}P]deoxyoligonucleotide probe homologous to domain I of previously cloned neuronal α_1 subunits. Of seventeen clones identified as α_{1A} types, the complete DNA sequence of the single 7.2 kb $\alpha_{1A\text{-}b}$ cDNA was determined on both strands. The $\alpha_{1A\text{-}b}$ (–V) construct was made by substituting a 2.4-kb *Xho* I/*Nhe* I fragment of $\alpha_{1A\text{-}a}$ into $\alpha_{1A\text{-}b}$. The $\alpha_{1A\text{-}a}$(+V) construct was made by substituting a 1.8-kb *Tth* III1 fragment of $\alpha_{1A\text{-}b}$ into $\alpha_{1A\text{-}a}$. The $\alpha_{1A\text{-}a}$ (+NP) cDNA was constructed by substituting a 2.5-kb *BamH*I fragment from $\alpha_{1A\text{-}b}$ into $\alpha_{1A\text{-}a}$. The $\alpha_{1A\text{-}b}$ (–NP) construct was created by switching the 2.5-kb fragment from $\alpha_{1A\text{-}a}$ into $\alpha_{1A\text{-}b}$. Chimeric cDNAs were originally constructed in the plasmid Bluescript and then subcloned into the *Xho* I/*Spe* I sites of the nuclear expression vector, pMT2. Each construct was verified by DNA sequencing across the chimera junctions and through the altered region.

To examine domain I–II linker splice junctions, we screened a rat genomic library (lambda DASH, Stratagene) using a [^{32}P]-labeled cDNA fragment to the $\alpha_{1A\text{-}a}$ domain I–II linker. A 5.2-kb *EcoR*I fragment that hybridized to oligonucleotide probes specific for α_{1A} sequences at positions 1200 and 1275 bp was selected and DNA sequencing used to identify the intron–exon boundaries across the I–II linker. Splicing in domain IV was analyzed by using PCR to amplify rat genomic sequences flanking S3 and S4. Direct sequencing of the PCR products identified the intron–exon boundaries.

For PCR detection of V_{421}, a sense oligonucleotide common to both $\alpha_{1A\text{-}a}$ and $\alpha_{1A\text{-}b}$ variants was used in conjunction with an antisense oligonucleotide containing the antisense sequence for Val_{421} at its 3′ end. *In situ* localization was done using 30 μm paraformaldehyde-fixed sections from 250 to 300 gm adult male rat brains. Sections were hybridized overnight at 37°C in 50% formamide, 0.6 M NaCl, 1 mM EDTA, 100 mM DTT, 10 mM Tris pH 7.5, 1× Denhardts, 10% dextran sulphate, 0.1% SDS, 0.1% sodium thiosulphate, 0.05% denatured salmon sperm DNA and 0.05% yeast tRNA. Probes consisted of [α-^{35}S]dATP end-labeled antisense 39-base synthetic deoxyoligonucleotides derived from the unique EF hand regions of $\alpha_{1A\text{-}a}$ and $\alpha_{1A\text{-}b}$. Sections were washed at 50°C in 0.5× SSC, 1% sodium thiosulphate and 14 mM β-mercaptoethanol, exposed to X-ray film for 1 week, then dipped in Kodak photographic emulsion NTB-2 and exposed for 2–4 weeks.

Acknowledgements

We thank M. Gilbert and A. Stea for comments, E. Perez-Reyes for β_{2a} and β_4 subunit cDNAs, and M. Ahlijanian (Pfizer) for ω-agatoxin IVA. T.W.S. was supported by a fellowship from the University of Singapore, Institute of Molecular Biology, E.B. by fellowships from INSERM and EMBO, K.S. by a grant from the Amytrophic Lateral Sclerosis Society of Canada, G.W.Z .by a grant from the Medical Research Council (MRC) of Canada and scholarships from MRC and the Alberta Heritage Foundation for Medical Research. E.B. and G.W.Z. are supported by NATO grant (CRG 971546) and T.P.S. is supported by a grant from the MRC of Canada and an MRC Scientist award.

Received 10 December 1998; accepted 25 March 1999

1. McCleskey, E. W. & Schroder, J. E. Functional properties of voltage–dependent calcium channels. *Curr. Top. Membr.* 39, 295–326 (1991).
2. Huguenard, J. R. Low–threshold calcium currents in central neurons. *Annu. Rev. Physiol.* 58, 329–348 (1996).
3. Murphy, T. J., Worley, P. F. & Baraban, J. M. L-type voltage-sensitive calcium channels mediate synaptic activation of immediate early genes. *Neuron* 7, 625–635 (1991).
4. Bading, H., Ginty, D. D. & Greenberg, M. E. Regulation of gene expression in hippocampal neurons by distinct calcium signaling pathways. *Science* 260, 181–186 (1993).
5. Turner, T. J., Adams, M. E. & Dunlap, M. E. Calcium channels coupled to glutamate release identified by ω-Aga-IVA. *Science* 258, 310–313 (1992).
6. Takahashi, T. & Momiyama, A. Different types of calcium channels mediate central synaptic transmission. *Nature* 366, 156–158 (1993).
7. Regehr, W. G. & Mintz, I. M. Participation of multiple calcium channel types in transmission at single climbing fiber to Purkinje cell synapses. *Neuron* 12, 605–613 (1994).
8. Dunlap, K., Luebke, J. I. & Turner, T. J. Exocytotic Ca^{2+} channels in mammalian central neurons. *Trends Neurosci.* 18, 89–98 (1995).
9. Stea, A., Soong, T. W. & Snutch, T. P. in *Handbook of Receptors and Channels: Ligand- and Voltage-Gated Ion Channels* (ed. North, R. A.) 113–152 (CRC Press, Boca Raton, Florida, 1995).

10. Soong, T. W. *et al.* Structure and functional expression of a member of the low voltage-activated calcium channel family. *Science* 260, 1133–1136 (1993).
11. Bourinet, E. *et al.* The α_{1E} calcium channel exhibits permeation properties similar to low-voltage-activated calcium channels. *J. Neurosci.* 16, 4983–4993 (1996).
12. Williams, M. E. *et al.* Structure and functional characterization of neuronal α_{1E} calcium channel subtypes. *J. Biol. Chem*. 269, 22347–22357 (1994).
13. Perez-Reyes, E. *et al.* Molecular characterization of a neuronal low-voltage-activated T-type calcium channel. *Nature* 391, 896–900 (1998).
14. Lee, J.-H. *et al.* Cloning and expression of a novel member of the low voltage-activated T-type calcium channel family. *J. Neurosci.* 19, 1912–1921 (1999).
15. Llinas, R., Sugimori, M., Lin, J. W. & Cherksey, B. Blocking and isolation of a calcium channel from neurons in mammals and cephalopods utilizing a toxin fraction (FTX) from funnel-web spider poison. *Proc. Natl. Acad. Sci. USA* 86, 1689–1693 (1989).
16. Mintz, I. M. *et al.* P-type calcium channels blocked by the spider toxin ω-Aga-IVA. *Nature* 355, 827–829 (1992).
17. Mintz, I. M., Adams, M. E. & Bean, B. P. P-type calcium channels in rat central and peripheral neurons. *Neuron* 9, 85–95 (1992).
18. Zhang, J.-F. *et al.* Distinctive pharmacology and kinetics of cloned neuronal Ca^{2+} channels and their possible counterparts in mammalian CNS neurons. *Neuropharmacology* 32, 1075–1080 (1993).
19. Randall, A. & Tsien, R. W. Pharmacological dissection of multiple types of Ca^{2+} channel currents in rat cerebellar granule neurons. *J. Neurosci.* 15, 2995–3012 (1995).
20. Wheeler, D. B., Randall, A. & Tsien, R. W. Roles of N-type and Q-type Ca^{2+} channels in supporting hippocampal synaptic transmission. *Science* 264, 107–111 (1994).
21. Tottene, A., Moretti, A. & Pietrobon, D. Functional diversity of P-type and R-type calcium channels in rat cerebellar neurons. *J. Neurosci.* 16, 6353–6363 (1996).
22. Forsythe, I. D., Tsujimoto, T., Barnes-Davies, M., Cuttle, M. F. & Takahashi, T. Inactivation of presynaptic calcium current contributes to synaptic depression at a fast central synapse. *Neuron* 20, 797–807 (1998).
23. Mori, Y. *et al.* Primary structure and functional expression from complementary DNA of a brain calcium channel. *Nature* 350, 398–402 (1991).
24. Starr, T. V. B., Prystay, W. & Snutch, T. P. Primary structure of a calcium channel that is highly expressed in the rat cerebellum. *Proc. Natl. Acad. Sci. USA* 88, 5621–5625 (1991).
25. Stea, A. *et al.* The localization and functional properties of a rat brain α_{1A} calcium channel reflect similarities to neuronal Q- and P-type channels. *Proc. Natl. Acad. Sci. USA* 91, 10576–10580 (1994).
26. Sather, W. A. *et al.* Distinctive biophysical and pharmacological properties of Class A (BI) calcium channel α_1 subunits. *Neuron* 11, 291–303 (1993).
27. Ophoff, R. A. *et al.* Familial hemiplegic migraine and episodic ataxia type-2 are caused by mutations in the Ca^{2+} channel gene CACNL1A4. *Cell* 87, 543–552 (1996).
28. Fletcher, C. F. *et al.* Absence epilepsy in tottering mutant mice is associated with calcium channel defects. *Cell* 87, 607–617 (1996).
29. Zhuchenko, O. *et al.* Autosomal dominant cerebellar ataxia (SCA6) associated with small polyglutamine expansions in the α_{1A}–voltage-dependent calcium channel. *Nat. Genet.* 15, 62–69 (1997).
30. Pragnell, M. *et al.* Calcium channel β subunit binds to a conserved motif in the I-II cytoplasmic linker of the α_1 subunit. *Nature* 368, 68–70 (1994).
31. Babitch, J. Channel hands. *Nature* 346, 321–322 (1990).
32. Zamponi, G. W. & Snutch, T. P. Modulation of voltage-dependent calcium channels by G proteins. *Curr. Opin. Neurobiol.* 8, 351–356 (1998).
33. Bean, B. P. Neurotransmitter inhibition of neuronal calcium channels by changes in channel voltage dependence. *Nature* 340, 153–156 (1989).
34. Stea, A., Soong, T. W. & Snutch, T. P. Determinants of PKC-dependent modulation of a family of neuronal calcium channels. *Neuron* 15, 929–940 (1995).
35. Yang, J., Ellinor, P. T., Sather,W. A., Zhang, J. F. & Tsien, R. W. Molecular determinants of Ca^{2+} selectivity and ion permeation in L-type Ca^{2+} channels. *Nature* 366, 158–161 (1993).
36. Nakai, J., Adams, B. A., Imoto, K. & Beam, K. G. Critical roles of the S3 segment and S3–S4 linker of repeat I in activation of L-type calcium channels. *Proc. Natl. Acad. Sci. USA* 91, 1014–1018 (1994).
37. Zhang, J.-F., Ellinor, P. T., Aldrich, R. W. & Tsien, R. W. Molecular determinants of voltage-dependent inactivation in calcium channels. *Nature* 372, 97–100 (1994).
38. Tanabe, T., Beam, K. G., Adams, B. A., Niidome, T. & Numa, S. Region of the skeletal muscle dihydropyridine receptor critical for excitation-contraction coupling. *Nature* 346, 567–569 (1990).
39. McDonough, S. I., Mintz, I. M. & Bean, B. P. Alteration of P-type calcium channel gating by the spider toxin ω-Aga-IVA. *Biophys. J.* 72, 2117–2128 (1997).
40. Rogers, J. C., Qu, Y., Tanada, T. N., Scheuer, T. & Catterall, W. A. Molecular determinants of high affinity binding of α-scorpion toxin and sea anemone toxin in the S3–S4 extracellular loop in domain IV of the Na^+ channel α subunit. *J. Biol. Chem*. 271, 15950–15962 (1996).
41. Cestele, S. *et al.* Voltage sensor trapping: enhanced activation of sodium channels by β-scorpion toxin bound to the S3–S4 loop in domain II. *Neuron* 21, 919–931 (1998).
42. Swartz, K. J & MacKinnon, R. Mapping the receptor site for hanatoxin, a gating modifier of voltage-dependent K^+ channels. *Neuron* 18, 675–682 (1997).
43. Li-Smerin, Y. & Swartz, K. J. Gating modifier toxins reveal a conserved structural motif in voltage-gated Ca^{2+} and K^+ channels. *Proc. Natl. Acad. Sci. USA* 95, 8585–8589 (1998).
44. Herlitze, S., Hockerman, G. H., Scheuer, T. & Catterall, W. A. Molecular determinants of the inactivation and G protein modulation in the intracellular loop connecting domains I and II of the calcium channel α_{1A} subunit. *Proc. Natl. Acad. Sci. USA* 93, 1512–1516 (1997).
45. Berrow, N. S., Brice, N. L., Tedder, I., Page, K. M. & Dolphin, A. C. Properties of cloned rat α1A calcium channels transiently expressed in the COS-7 cell line. *Eur. J. Neurosci.* 9, 739–748 (1997).
46. Buller, A. L. & White, M. M. Altered patterns of glycosylation of the *Torpedo* acetylcholine receptor expressed in *Xenopus* oocytes. *J. Membrane Biol.* 115, 179–189 (1990).
47. Westenbroeck, R. E. *et al.* Immunochemical identification and subcellular distribution of the α_{1A} subunits of brain calcium channels. *J. Neurosci.* 15, 6403–6418 (1995).
48. Brody, L. D., Patil, P. G., Mulle, J. G., Snutch, T. P. & Yue, D. Y. Burst of action potential waveforms relieve G-protein inhibition of recombinant P/Q-type Ca^{2+} channels in HEK 293 cells. *J. Physiol. (Lond.)* 499, 637–644 (1997).
49. Ligon, B., Boyd, A. E. III & Dunlap, K. Class A calcium channel variants in pancreatic isets and their role in insulin secretion. *J. Biol. Chem.* 273, 13905–13911 (1998).
50. Yu, A. S., Herbert, S. C., Brenner, B. M. & Lytton, J. Molecular characterization and nephron distribution of a family of transcripts encoding the pore-forming subunit of Ca^{2+} channels in the kidney. *Proc. Natl. Acad. Sci. USA* 89, 10494–10498 (1992).